45. C. Matyas, in *Past and Future Rapid Environmental Changes: The Spatial and Evolutionary Responses of Terrestrial Biota*, B. Huntley *et al.*, Eds. (Springer-Verlag, Berlin, 1997), pp. 357–370.
46. B. Huntley, I. C. Prentice, in *Global Climates Since the Last Glacial Maximum*, H. E. Wright Jr. *et al.*, Eds. (Univ. of Minnesota Press, Minneapolis, MN, 1993), pp. 136–168.
47. G. Eriksson, S. Andersson, V. Eiche, J. Ifver, A. Persson, *Stud. For. Suecica* **156**, 1 (1980).
48. J. Mikola, *Silv. Fenn.* **16**, 178 (1982).
49. U. Gullberg, R. Yaxdani, D. Rudin, N. Ryman, *Silvae Genet.* **34**, 193 (1985).
50. G. R. Furnier, M. Stine, C. A. Mohn, M. A. Clyde, *Can. J. For. Res.* **21**, 707 (1991).
51. R.-C. Yang, F. C. Yeh, A. D. Yanchuk, *Genetics* **142**, 1045 (1996).
52. J. S. Clark *et al.*, *Bioscience* **48**, 13 (1998).
53. L. F. Pitelka, Plant Migration Workshop Group, *Am. Sci.* **85**, 464 (1997).
54. M. Lynch, R. Lande, in *Biotic Interactions and Global Change* P. M. Kareiva, J. G. Kingsolver, R. B. Huey, Eds (Sinauer Associates, Sunderland, MA, 1993), pp. 235–250.
55. K. V. Walker, M. B. Davis, S. Sugita, personal communication.
56. J. C. Ritchie, G. M. MacDonald, *J. Biogeogr.* **13**, 527 (1986).
57. J. R. Etterson, personal communication.
58. D. S. Falconer, T. F. C. Mackay, *Introduction to Quantitative Genetics* (Longman, Essex, UK, 1996).
59. J. R. Etterson, R. G. Shaw, personal communication.
60. J. Antonovics, *Ann. Mo. Bot. Garden* **63**, 224 (1976).
61. N. Miyoshi, T. Fujiki, Y. Morita, *Rev. Palaeobot. Palynol.* **104**, 267 (1999).
62. M. Tsukada, in *Vegetation History*, B. Huntley, T. Webb III, Eds. (Kluwer Academic, Dordrecht, Netherlands, 1988), pp. 459–518.
63. A. D. Bradshaw, *Philos. Trans. R. Soc. London B Biol. Sci.* **333**, 289 (1991).
64. S. Jackson, C. Weng, *Proc. Natl. Acad. Sci. U.S.A.* **96**, 13847 (1999).
65. G. Jacobson, T. Webb III, E. C. Grimm, in *North America and Adjacent Oceans During the Last Deglaciation*, W. F. Ruddiman, H. E. Wright Jr., Ed. (Geological Society of America, Boulder, CO, 1987), pp. 277–288.
66. W. G. Spaulding, E. B. Leopold, T. R. Van Devender, in *Late-Quaternary Environments of the United States*, vol. 1, *The Late Pleistocene*, S. C. Porter, Ed. (Univ. of Minnesota Press, Minneapolis, MN, 1983), pp. 259–293.
67. M. Tsukada, *Bot. Mag. Tokyo* **95**, 203 (1982).
68. We are very grateful to C. Douglas for preparing the figures for the paper. We also thank the following for helpful criticism of the manuscript: C. Douglas, D. Lytle, K. McLauchlan, G. Wahl, S. Halpern, E. Lonsdorf, R. Zink, G. May, S. Chang, J. Hill, J. Antonovics, and three anonymous reviewers. This work was supported by the NSF.

REVIEW

Sea Level Change Through the Last Glacial Cycle

Kurt Lambeck*and John Chappell

Sea level change during the Quaternary is primarily a consequence of the cyclic growth and decay of ice sheets, resulting in a complex spatial and temporal pattern. Observations of this variability provide constraints on the timing, rates, and magnitudes of the changes in ice mass during a glacial cycle, as well as more limited information on the distribution of ice between the major ice sheets at any time. Observations of glacially induced sea level changes also provide information on the response of the mantle to surface loading on time scales of 10^3 to 10^5 years. Regional analyses indicate that the earth-response function is depth dependent as well as spatially variable. Comprehensive models of sea level change enable the migration of coastlines to be predicted during glacial cycles, including the anthropologically important period from about 60,000 to 20,000 years ago.

Sea levels have fluctuated throughout geological time, periodically encroaching or retreating across coastal plains. Changes in the relative positions of sea and land surfaces are indicative of vertical movements of the land, changes in ocean volume, or, in most cases, of both. Figure 1 illustrates examples of observed sea level change on different time scales, from about 10^8 years to 1 year. Global changes occur on time scales of millions of years, with amplitudes on the order of several hundred meters (*1*, *2*) (Fig. 1A) and are associated mainly with plate tectonics–induced changes in ocean basin geometry. During the Quaternary, the dominant contribution to sea level change has been the periodic exchange of mass between ice sheets and oceans: ice ages being times of sea level lowstands and interglacials being times of relative highstands. Figure 1B gives a representative result of relative sea level change during the last glacial cycle as recorded in reef sequences of the Huon Peninsula, Papua New Guinea. Superimposed on the global signals are more regional and local changes caused by uplift and subsidence of the coastal zone or by changes in regional and local climate. At decadal, annual, and shorter intervals (Fig. 1C), the climate-, meteorology-, and tide-driven changes become important. Observations of sea level change also indicate considerable spatial variation. This is illustrated in Fig. 2 for a number of tectonically stable sites or, as in the case of Barbados, for sites where it is possible to correct for tectonic uplift. The observed signals vary substantially from site to site, even when the localities lie relatively near to each other such as the Scandinavian Ångerman and Andøya sites: At the first site, sea level has fallen nearly 200 m in the past 9000 years, whereas at the second, the level 9000 years ago was near the present level. In contrast, at Barbados, sea level was about 30 m below the present level at that time. In southern England, levels have risen slowly over the past 7000 years, but along the Australian margin they have fallen by a few meters during the same interval. The relative sea level change therefore exhibits complex temporal and spatial patterns that contain information about a range of Earth and climate processes.

Understanding this time-space variability is pertinent to a number of scientific disciplines. The glacial signal not only provides a boundary condition on changes in ice sheets [both on the mass of ice and on the timing of past glaciations (*3*–*6*)] but also on the isotopic composition of the ice. Some of the spatial variability seen in the observational record is the result of Earth's adjustment to changing ice loads, and this signal contains information about the viscosity of the mantle (*5*, *7*, *8*). If the glacially induced changes are known, the paleo–sea level information provides estimates of the rates of vertical tectonic movements (*9*) and constraints on tectonic processes. Once comprehensive sea level models are developed, it becomes possible to test hypotheses about the migrations of flora and fauna across shallow seas that are now covered by the ocean. Finally, to understand future sea level rise, the background "natural" signal must be known (*10*). Many of the factors contributing to changes in sea level are linked, either through physical processes or through observational evidence, and the success of the outcomes of the various sea level studies depends very much on the ability to separate the different contributions to the observational record.

Research School of Earth Sciences, The Australian National University, Canberra 0200, Australia.

*Also The Swedish Research Council 2001 Tage Erlander Professor, Lund University, Sweden.

Observational Evidence

Evidence for past sea level change occurs mostly in the form of raised or submerged shorelines, indicated by, for example, fossil coral reefs above their present growth positions or submerged in situ tree stumps. The observations usually form limiting values only: The sea level must have been lower than the tree roots at the time of their growth, and it must have been higher than the reef at the time of coral growth (*11*). The results in Fig. 2 are representative of the principal materials used to identify past sea levels. The Andøya result (*12*) is based on peats and sediments in shallow elevated basins that at some past time were in contact with the sea. Transitions from freshwater to marine deposits are indicative of marine flooding of the basin and of a relative rise in sea level, whereas the reverse sequence is indicative of a fall in level. Series of these isolation basins at different present-day elevations then yield detailed patterns of regional sea level change. The timing of the transgressions and regressions is established by radiocarbon dating of materials deposited near the transition. The Ångerman result (*13*) is from deltaic sediments that now occur up to 200 m above the present sea level. The time scale in this case has been determined by counting annual laminations in the total sequence of seasonal deposits—varves—recorded continuously in the delta sequences from late glacial times up to the present. The southern England data (*14*) consist of submerged freshwater-estuarine transition peats and in situ tree roots. For the latter, a question is what is the relationship between the local water table, whose rise terminates tree growth, and mean sea level. The Sunda Shelf evidence (*15*) is a mix of indicators that establish the progressive flooding of this broad shelf during the last deglaciation. A question here is whether the sampled material represents in situ material or older material that was transported to the locality at a later time. The Barbados result is based on the age-depth relationship of fossil corals (*16*–*19*), and the question here is what was the water depth at the time of coral growth (*20*, *21*). An important feature of the coral material is that it can be dated by both radiocarbon and uranium-series methods, and it provides the basis for calibrating the radiocarbon time scale for the interval that is beyond the capabilities of varve and tree-ring chronologies (*22*). The North Queensland record for the past 7000 years is from micro-atoll formations of corals whose living counterparts in open-sea environments occur up to mean low-water spring tide to within 10 cm or less. They provide, therefore, a precise indicator of paleo–sea level, except that local changes on reef flats over time may result in "ponding," so that the corals grow to a level higher than that of their open-ocean counterparts (*23*, *24*).

These examples are indicative of some of the limitations of paleo–sea level indicators, but despite reservations about detail, well-developed patterns of change do emerge. For areas near the centers of former ice sheets, such as the Ångerman region or Hudson Bay of Arctic Canada (*25*), the pattern is one of falling sea level, from the time the sea first entered into the area until the present. The time series observed in Andøya is typical for margins of former ice sheets or centers of small ice sheets, such as over Scotland (*26*). The results for southern England are representative of broad zones beyond the former ice, including the Mediterranean Sea and the Atlantic and Gulf of Mexico coasts of the United States. The Sunda and Barbados results are representative of locations far from former ice margins (*27*), as is the Queensland result for the past 7000 years, with the small highstand in mid-Holocene time varying substantially from location to location (*28*, *29*).

Most of the available sea level data is for the period after the last deglaciation, because earlier records were mostly destroyed by rising sea levels at the onset of deglaciation or by advancing ice sheets during the lead-up to maximum glaciation. In areas of tectonic uplift, earlier records may be preserved when shorelines have been uplifted beyond the reach of the sea by the time the next highstand occurs. This is the case for the Huon Peninsula of Papua New Guinea, where major reef sequences occur up to 1000 m or more above the present sea level and each reef crest corresponds to a time when sea level rise and tectonic uplift were about equal. The lower part of the sequences, including submerged reefs, have been examined in detail (*30*–*35*), and it has been possible to establish the local sea level curve for the last glacial cycle illustrated in Fig. 1B (*36*, *37*). The Huon records continue to be important for calibrating less direct indicators of sea level change, such as marine oxygen isotope records (*33*, *38*), and for quantifying

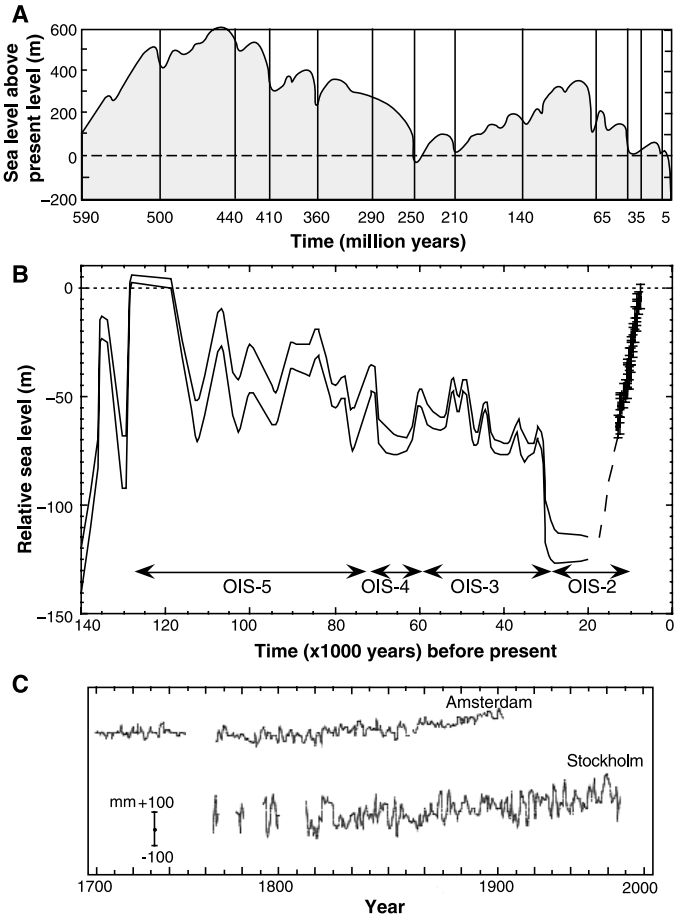

Fig. 1. Temporal variation in sea level at three time scales. (**A**) ~10^8 years as inferred from seismic sequence stratigraphy (*1*, *2*). The higher frequency change reflects a combination of global and local signatures, but the major oscillations are primarily global in origin, associated with continental breakup and the formation of new ocean ridge systems. (**B**) Relative sea level at Huon Peninsula, Papua New Guinea, for the past ~10^5 years inferred from the height-age relationships of raised reefs and from submerged fossil corals for the past 13,000 years (Fig. 3). The fluctuations are the result of the glacial cycle–induced changes in continental-based ice volumes. Upper and lower limits are shown for the pre-LGM part of the record (before about 25,000 years ago), and mean sea level estimates with error bars are shown for the post-LGM record. The LGM record is missing from Huon, and the dashed lines for this period correspond to information from northwestern Australia (Fig. 2). The timing and duration of the major oxygen isotope stages is shown. (**C**) Change on century-to-annual time scales as measured by tide gauges from Amsterdam and Stockholm. The latter record has had a secular fall of about 4 mm/year (attributed to glacial rebound) removed (*95*, *96*). These changes are primarily of climatic origin, and the apparent small secular change starting in the latter part of the 19th century is attributed to the impact of industrialization on climate (*10*).

some of the rapid changes in sea level in the period leading up to the Last Glacial Maximum (LGM) (*35*, *39*). Few corals from the older Huon Peninsula reefs have been accurately dated, although new results from elsewhere (*40*, *41*) suggest that this should be possible.

Glacial Isostasy

When ice sheets melt, the resulting sea level change is spatially variable because of the deformation of Earth's surface under the time-dependent ice and water load and because of the changing gravitational potential of the Earth-ocean-ice system. The combined deformation-gravitational effects are referred to as the glacio-hydro-isostatic contributions to sea level, and it is they that cause the spatial variability illustrated in Fig. 2. In a first approximation, sea level rises by an amount $\Delta\zeta_e(t)$ that relates to the land-based ice volume V_i according to

$$\Delta\zeta_e(t) = -\frac{\rho_i}{\rho_o}\int_t \frac{1}{A_o(t)}\frac{dV_i}{dt}\,dt \qquad (1)$$

where $A_o(t)$ is the ocean surface area and ρ_i, ρ_o are the average densities of ice and ocean water, respectively. $\Delta\zeta_e(t)$ is the ice-volume equivalent sea level change, or simply the equivalent sea level change. It equals eustatic change if no other factors contribute to changes in ocean volume. The relative sea level change $\Delta\zeta_{rsl}(\varphi, t)$ at position φ and time t, ignoring possible tectonic displacements of the coastal zone, is

$$\Delta\zeta_{rsl}(\varphi,t) = \Delta\zeta_e(t) + \Delta\zeta_i(\varphi,t) + \Delta\zeta_w(\varphi,t) \qquad (2)$$

where the $\Delta\zeta_i$ and $\Delta\zeta_w$ are the glacio- and hydro-isostatic contributions. Both are functions of position and time. The water depth or terrain height, expressed relative to coeval sea level, is

$$h(\varphi,t) = h(\varphi,t_0) - \Delta\zeta_{rsl}(\varphi,t) \qquad (3)$$

where $h(\varphi,t_0)$ is the present-day (t_0) bathymetry or topography at φ. Both isostatic terms in Eq. 2 are functions of Earth rheology as well as of fluctuations in the ice sheets over time.

In formerly glaciated areas, it is the glacio-hydro-isostatic term $\Delta\zeta_i$ that dominates during and after deglaciation. It results in an uplifting crust at a rate that exceeds the effect of the increasing ocean volume, so that sea level locally falls [the Ångerman result (Fig. 2)]. At the ice margin, this rebound is smaller than it is near the ice center, and although the rebound dominates initially, it is the equivalent sea level rise from more distant ice sheets that becomes important later. When all melting has ceased, the residual rebound determines the local sea level change (the Andøya result). During ice sheet growth, mantle material beneath the loaded area is displaced outward, and broad bulges develop around the loaded area. When the ice sheets, melt these bulges subside. This results in signals where, after an initially rapid rise, relative sea level continues to rise slowly, once melting has ceased (the southern England result). Much further from the ice, the water load becomes the dominant cause of planetary deformation (this is the hydro-isostatic contribution $\Delta\zeta_w$). Here the ocean floor is loaded by the

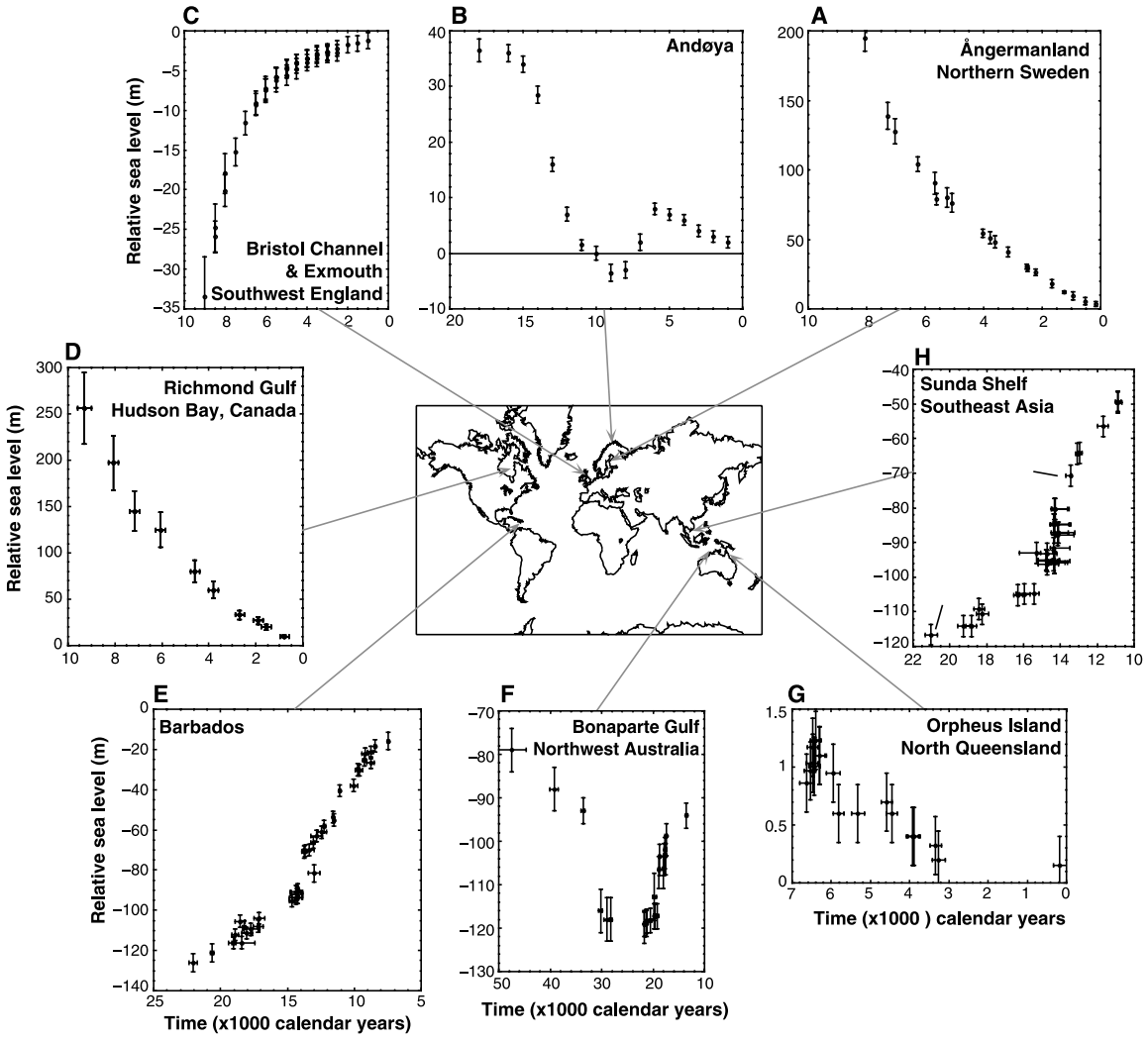

Fig. 2. Observed spatial variability of sea level change since the time of the LGM from tectonically stable areas or areas where the tectonic rate is known and has been removed from the observed signal. (**A**) Ångerman, Gulf of Bothnia, Sweden (*13*). (**B**) Andøya, Nordland, Norway (*12*). (**C**) South of England (*14*). (**D**) Hudson Bay, Canada (*4*). (**E**) Barbados (*16*–*18*). (**F**) Bonaparte Gulf, northwest Australia (*27*). (**G**) Orpheus Island, North Queensland, Australia [(*23*) and unpublished Australian National University data]. (**H**) Sunda Shelf, southeast Asia (*15*). Note the different time and amplitude scales. In the examples illustrated, all observed depths or elevations of the sea level indicators have been reduced to mean sea level. All time scales are in calendar years.

meltwater, producing subsidence of the sea floor and adjacent margins. This effect is most pronounced at continental margins far from the ice sheets, such as along the Australian coast, and once melting has ceased, sea levels continue to fall at a slow but perceptible rate. This produces the small highstands seen at the Queensland sites. Because the hydro-isostatic effect at a site depends on the distance from and distribution of the meltwater, the amplitudes of these highstands can vary substantially from site to site (*42*).

The theory used for predicting isostatic corrections (*43–51*) has been tested against independent formulations and numerical codes. The parameters that quantify the predictions describe the earth-response function and the surface loading history. Once the ice load is defined, the water load history is determined from knowledge of the ocean basin geometry, including the deformation of the basin over time and any movement of grounded ice across the shelves, subject to the conditions that ice and water mass is conserved and that the ocean surface remains a gravitational equipotential surface at all times. The modification of sea level by the time-dependent gravitational attraction between the solid earth, ocean, and ice is included, as is the effect of glacially induced changes in Earth rotation on sea level.

Ice Volumes Through the Last Glacial Cycle

The limits of the ice sheets at the time of the LGM and their subsequent retreat are well established for northern Europe and North America (*52–54*), but major uncertainties remain for other areas, such as eastern Siberia (*55*). Knowledge is also limited about the ice cover over shelf areas adjacent to the continental ice masses, such as the offshore limits of grounded Antarctic ice during the LGM (*52*, *56*). More uncertain still is the ice thickness at LGM and late glacial times. In a few instances, this has been measured directly from trimlines on nunataks that stood above the ice. But this has not been possible for the major North American and northern European ice sheets, and the estimates of ice thickness are dependent on assumptions about snow supply and ablation and about the nature of the rock-ice interface. Information about the growth and decay cycles of the ice sheets before the LGM is minimal, because the record was mostly destroyed by the advance and retreat of the last glacial cycle and because the materials that may have survived are too old for reliable radiocarbon dating.

The sea level signal at sites far from the former ice margins approximates the equivalent sea level function (Eq. 1) to within about 10 to 15%, and the isostatic contribution is mainly from the water loading, which is insensitive to the details of the ice sheets, provided that the total ice volumes are correct to within about 10 to 20%. Also, these contributions are not strongly dependent on Earth rheology within a broad range of values for lithospheric thickness and mantle viscosity (*29*). Hence, through an iterative procedure, it becomes possible to estimate changes in ice volumes V_i from observed sea levels $\Delta\zeta_{rsl}^{obs}$ according to

$$\Delta\zeta_e = \Delta\zeta_{rsl}^{obs} - (\Delta\zeta_i + \Delta\zeta_W) \qquad (4)$$

and Eq. 1. Figure 3 illustrates the resulting equivalent sea levels for the past 140,000 years (*57*). The post-LGM result is well established, with records from individual sites

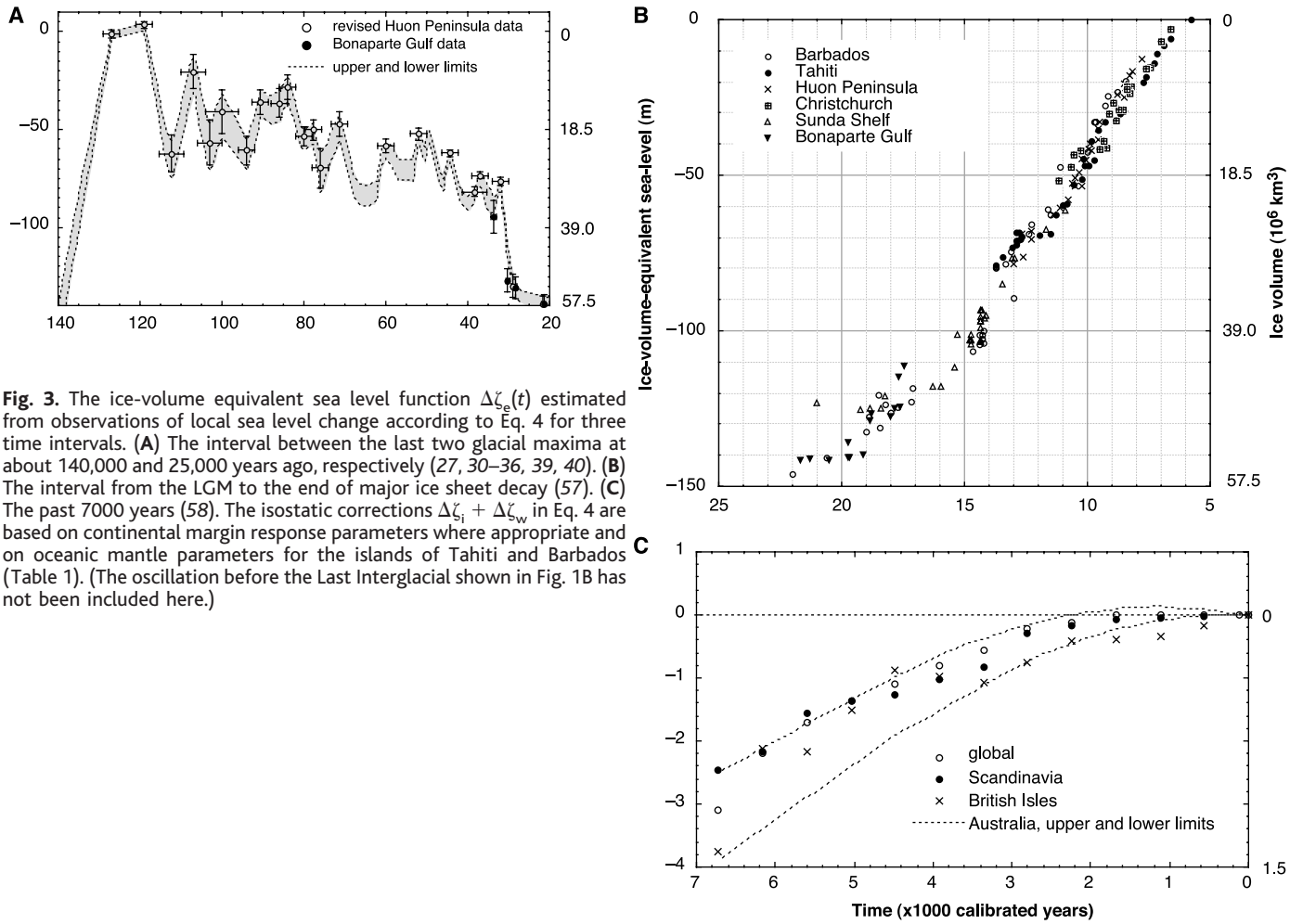

Fig. 3. The ice-volume equivalent sea level function $\Delta\zeta_e(t)$ estimated from observations of local sea level change according to Eq. 4 for three time intervals. (**A**) The interval between the last two glacial maxima at about 140,000 and 25,000 years ago, respectively (*27*, *30–36*, *39*, *40*). (**B**) The interval from the LGM to the end of major ice sheet decay (*57*). (**C**) The past 7000 years (*58*). The isostatic corrections $\Delta\zeta_i + \Delta\zeta_w$ in Eq. 4 are based on continental margin response parameters where appropriate and on oceanic mantle parameters for the islands of Tahiti and Barbados (Table 1). (The oscillation before the Last Interglacial shown in Fig. 1B has not been included here.)

giving concordant results within observational and modeling uncertainties. They indicate an irregular rate of glacial melting from the onset at about 19,000 years ago to the termination at about 7000 years ago. However, the rate of melting has been variable: In two periods of rapid and sustained sea level rise from about 16,000 to 12,500 and again from 11,500 to 8000 years ago, the rates of equivalent sea level rise approached 15 m in 1000 years (*16*, *17*, *31*). These two phases of sea level rise appear to have been separated by a short interval when sea levels remained constant; if substantiated by future data sets, this suggests that the Younger Dryas interval was a period of global cessation of ice retreat. By 7000 years ago, ocean volumes had approached their present day levels, but a small increase in ocean volume appears to have occurred until more recent times (*3*, *58*). Because the northern ice sheets had largely vanished by 7000 years ago, this is suggestive of a small ongoing melting of parts of the Antarctic ice sheet (*3*, *59*).

The earlier part of the record indicates that sea levels fell rapidly toward the LGM lowstand about 30,000 years ago. Thus, if the LGM is defined by the timing of maximum global ice volumes, then this interval lasted about 10,000 years, which is longer than the interval usually inferred from the benthic foraminifera oxygen isotope record (*60*). Furthermore, the pre-LGM period is characterized by substantial fluctuations in sea level of 10 to 15 m about every 6000 years. The timing of these rapid change events during oxygen isotope stage 3 (OIS–3) apparently coincides with Heinrich ice-rafting events recorded in North Atlantic sediments (*61*), which suggests that they reflect major ice discharges from continent-based or shelf-grounded ice sheets (*62*). Of note is that sea level falls during this period occur in similarly short time intervals and that ice accumulation also appears to have been a rapid process (*39*).

Table 1. Estimates for earth response parameters (with effective lithospheric thickness H_1 and effective viscosities η_{um}, η_{lm} for the upper and lower mantle) for three different regions. The continental mantle solution is based on sea level analyses for northern Europe (*8*, *51*, *73*), with the last solution including global rotational constraints for constraining lower mantle viscosity. The continental margin results are based on the analysis of the late Holocene data from Australia (*29*, *58*). The oceanic result is a solution of Pacific sea levels in which the lower mantle viscosity has been constrained to the value in parentheses (*80*).

Model	H_1 (km)	η_{um} ($\times 10^{20}$ Pa·s)	η_{lm} ($\times 10^{22}$ Pa·s)
Continental mantle	65–85	3–5	0.5–3
Continental margin mantle	65–80	1.5–2.5	0.5–3
Oceanic mantle	~50	~1	(1)

What the equivalent sea level results do not reveal is where the ice was located. Rebound data from within former ice margins provide some constraint on the ice volumes of individual ice sheets, and solutions for LGM and late glacial ice volumes suggest that the maximum ice thickness over North America and Europe is unlikely to have exceeded about 2000 to 2500 m (*4*, *8*). This leads to a total Northern Hemisphere ice mass that is less than that required to explain the global estimates inferred from the equivalent sea level function and to the conclusion that Antarctic ice volumes were greater at the LGM than they are today by 25 to 30 m of equivalent sea level. Rebound analyses from sparse data from the Antarctic margin support a post-LGM reduction in ice volume, but the field data are inadequate for complete analyses (*63*, *64*). In particular, because the observational records postdate the ice retreat, the early part of the ice load for both hemispheres is not well constrained (*6*, *65*), and the distribution between individual ice sheets of the total LGM ice volume inferred from the distal sites remains unsatisfactory.

Figure 3 also indicates the change in volume of ice throughout the last glacial cycle relative to the present-day ice volume. This volume includes all grounded ice, including ice on the shelves that displaced seawater. The excess ice at the LGM is about 5.2×10^7 km^3, which is about 5% greater than the glaciological lower estimate established by the Climate: Long-range Investigation, Mapping, and Prediction (CLIMAP) project but 30% less than CLIMAP's upper limit estimate (*66*). From the mean isotopic $\delta^{18}O$ composition of seawater at the LGM, that of the excess ice is $(\rho_i/\rho_o)\ V_{i,t}\ \delta^{18}O_{i,t} = V_{o,0}\ \delta^{18}O_{o,0} - V_{o,t}\ \delta^{18}O_{o,t}$, where $V_{i,t}$, $\delta^{18}O_{i,t}$ and $V_{o,t}$, $\delta^{18}O_{o,t}$ are the volumes and oxygen isotopic compositions of the excess ice and the oceans at the LGM, and $V_{o,0}$, $\delta^{18}O_{o,0}$ are the corresponding present-day values. Recent data (*67*, *68*) from deep sea sediments indicate that $\delta^{18}O_{o,t}$ of seawater at the time of the LGM was about 1 ± 0.1 per mil (‰) higher than today, and with a present ocean volume $V_{o,0} = 1.37 \times 10^9$ km^3, the globally averaged $\delta^{18}O_{i,t}$ is about –27‰. With 20 to 25% of the excess ice located in Antarctica, where ice cores show LGM isotopic compositions of around –50‰, the average bulk composition of the Northern Hemisphere LGM ice must have been about –20‰. This is significantly heavier than that of LGM Greenland ice (≈ –40‰) (*69*), which suggests that the precipitation that nourished much of the LGM ice sheet was isotopically less depleted than that falling at the higher latitudes of Greenland.

Mantle Viscosity

The viscous response of the mantle to changes in surface loads is documented by numerous geophysical and geological observations, including the relative sea level changes themselves (*70*). Laboratory experiments at representative mantle temperatures indicate that terrestrial materials deform nonlinearly when exposed to stress, but linear viscoelastic models appear to be adequate for describing observed glacial rebound phenomena. Thus, over the range of stress differences and time scales representative of glacial rebound (~30 MPa and 10^3 to 10^5 years, respectively), the mantle effectively behaves as a linear viscoelastic body. Geological and geophysical observations also indicate that the uppermost part of Earth, the lithosphere, responds elastically to surface loads of long duration (~10^6 years), even when the load-induced stress in the underlying mantle has relaxed. Hence, a viscoelastic mantle with overlying elastic lithosphere provides a good first-order description of the planet's response to glacial loads. The depth dependence of the elastic parameters, as well as of density, are established from seismic models of radial Earth structure, but the viscosity profile is parameterized and, in some cases along with the effective thickness of the lithosphere, is included as unknown in the inversion of rebound and related data (*5*, *7*, *8*, *51*, *71*).

The principal questions about the resulting effective viscosity are whether it is depth dependent and whether it is spatially variable. Answers come largely from the glacial rebound analysis itself, because there is as yet no satisfactory theory for Earth's interior that allows the viscosity structure to be predicted from ab initio considerations. What is important in inversions of sea level data for mantle viscosity is that considerable trade off can occur between viscosity and lithospheric thickness. For example, in some solutions the lithospheric thickness has been set to an a priori value of 120 to 125 km (*4*, *5*, *7*, *71*), but this may lead to estimates for upper mantle viscosity that are higher than if both this viscosity and lithospheric thickness are considered as unknowns in the inversion (*72*, *73*). The depth dependence of the effective mantle viscosity has been well established, with the average viscosity for the lower mantle exceeding that of the upper mantle by a factor of 50 to 100 (*8*, *73–75*), which is consistent with independent estimates based on inversions of geoid and seismic tomographic data (*75–77*). Depth dependence of the viscosity has also been identified within the upper mantle (above about 670 km depth) (*5*, *51*, *73*).

Models of upper mantle structure from the

inversion of seismic shear wave or attenuation data indicate that lateral variation in material properties occurs (*78*) and that corresponding variations in mantle temperature and hence upper mantle viscosity can be expected. Operational models for glacial rebound with lateral mantle structure do not yet exist, and it is questionable whether the observational data base is adequate for global inversions for both lateral and depth variation in mantle response when, at the same time, there remain uncertainties about the ice load history. Thus, in the absence of global solutions for a laterally variable mantle response, an alternate strategy is to carry out regional solutions and to seek viscosities that are representative of regional mantle conditions only (*79*).

Table 1 summarizes representative results for three-layered models corresponding to three different regions: Scandinavia, Australia, and the southern Pacific. In the first two solutions, the search has been conducted within broad limits of the three parameters, and the solutions indicate that lateral variability in effective upper mantle viscosity may be important. For continental-margin Australia, the isostatic effect is primarily the result of the response to water loading, with a flow of mantle material from beneath the ocean lithosphere to beneath the continental lithosphere. The resulting upper mantle viscosity is representative, therefore, of average ocean and continental mantle values. In contrast, the Fennoscandian rebound largely reflects mantle flow beneath the continental lithosphere. For only a few localities is there sufficient field evidence that enables regional response parameters to be estimated, but, in a first approximation, the two regional results indicate that oceanic mantle viscosity is less than continental mantle viscosity. This is consistent with known thermal and seismic wave propagation differences between the two regions as well as with some preliminary sea level analyses for Pacific island regions (*80*). This result has as consequence that when estimating past ice volumes from sea level data for different localities, different parameters may need to be used according to the representative mantle conditions. This has been done for the results illustrated in Fig. 3, where "continental margin" parameters have been used for the Huon, Bonaparte, and Sunda observations and "oceanic" parameters have been used for Tahiti and Barbados.

Shoreline Reconstructions

At one level, the isostatic rebound model can be seen as an interpolation device for predicting sea level change from spatially and temporally incomplete observational evidence. The real challenge lies in the interpretation of the effective parameters introduced to describe the earth response and load history. But for predicting the course of shorelines through time, this latter step is not important provided that the parameters are internally consistent with the fragments of available observations. With the schematic sea level equation (Eq. 2) solved, water depths at any time in the past follow from Eq. 3, and the paleo shorelines at time t correspond to the contours $h(\varphi, t) = 0$. Thus, provided that the present-day shallow water bathymetry is known with high resolution, it becomes possible to examine the migrations of shorelines through time for intervals for which sufficient observational data exist to constrain the isostatic variables. Predictions of shorelines since the time of the LGM have been published for both global (*81*) and regional reconstructions (*82*–*84*), and these can provide useful insights into the interpretation of prehistoric sites. For example, an absence of fish bones in the Late Palaeolithic strata of Franchthi Cave in Greece may have as much to do with the shoreline being far away at that time than with the evolution of fishing skills (*83*, *85*, *86*). Likewise, the gradual transformation of a broad valley with large freshwater lakes and a major river system into a submerged Persian Gulf from the LGM to about 8000 years ago may well have been a powerful factor in human migrations during the period, leading up to the pre-Sumerian settlements in lower Mesopotamia (*84*, *87*, *88*).

The timing of the flooding of the Bass Strait between the Australian mainland and Tasmania similarly provides an important input into the debate about early human movements in pre-LGM times (*89*–*91*). The debate here concerns the first arrival of humans in Tasmania as compared to their first occupation of other southern regions of the continent. The

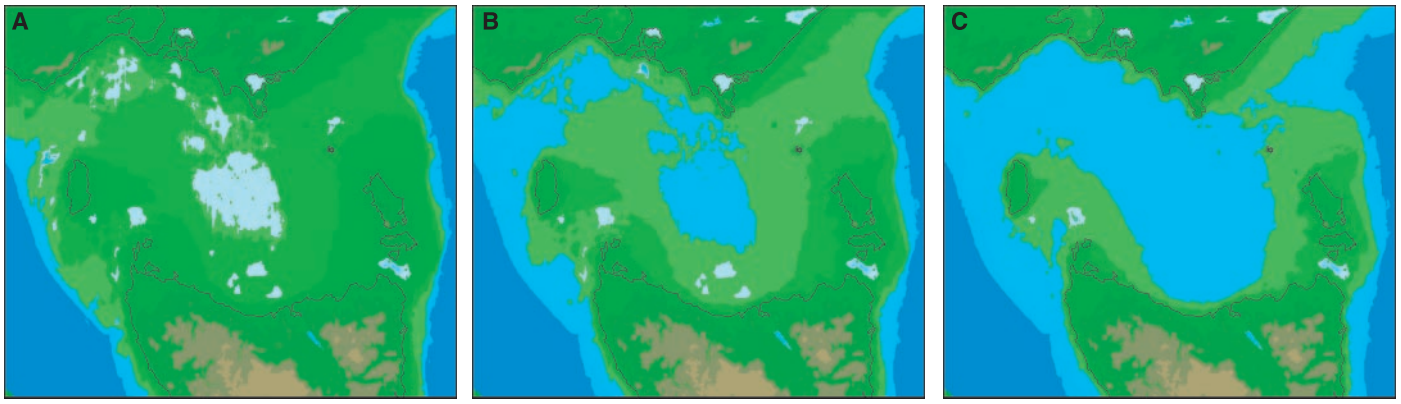

Fig. 4. Shoreline reconstructions for the Bass Strait between mainland Australia and Tasmania. This shallow sea was above sea level during times of lowstand but was periodically inundated during the time of human occupation of Australia. The lowest two land contours, identified by changes in shades of green, correspond to 25 and 50 m above sea level. The pale blue areas denote freshwater or marshy depressions. (**A**) At the peak of the last glaciation, 25,000 years ago. (**B**) At 17,500 years ago, when the relative sea level had risen sufficiently for it to enter the Bass basin from the west (the western sill) and form an estuarine environment. (**C**) At 14,000 years ago, when the sea level rise reached the barrier in the east and Tasmania became isolated from the Australian mainland. These model reconstructions assume that tectonic movements of the sea floor have been negligible during the last glacial cycle and that any erosion of, or sedimentation on, the sea floor has been insignificant. (**D**) The change in elevation, with respect to coeval sea level, of the lowest points (the sill locations) for the land bridges between the mainland and Tasmania, to the east and west of the central depression. The interval between 40,000 and 36,000 years corresponds to the time of the first known human occupation of Tasmania.

oldest human occupation site in Tasmania has been dated at ~36,000 to 40,000 calendar years (*91*), compared with about 56,000 to 68,000 years at Lake Mungo in southeastern Australia (*92*, *93*), and a question that has been raised is whether the Bass Strait provided a barrier to earlier occupation of Tasmania. Figure 4 illustrates the reconstruction of this waterway at the LGM and at two post-LGM critical periods. At the height of the last glaciation (Fig. 4A), the strait was exposed, with a large depression in its center connected but inaccessible to the southern ocean via a low and broad valley. During the subsequent deglaciation, the sea first entered this depression from the west at about 17,500 years ago (Fig. 4B), and the eastern land connection was broken about 3500 years later (Fig. 4C), leaving Tasmania isolated from the Australian mainland. The locations where these separations occur also determine the separations for earlier periods, and the predicted minimum elevations (Eq. 3) for the eastern and western land connections is given in Fig. 4D. (The error bars on these sill elevations are similar to those in Fig. 3A.) This indicates that Tasmania was isolated from mainland Australia from the time of the penultimate deglaciation at about 135,000 years ago until about 43,000 years ago, with the exception of several short periods when an eastern land connection may have existed (at ~76,000, 68,000 to 62,000, and 46,000 years ago). At any of these times, this land bridge would have been tenuous (with elevations only about 5 m above the coeval sea level), largely devoid of vegetation, and susceptible to flooding at times of high seas and storms. The first sustained land connection on the eastern side occurred at about 43,000 years ago, at which time the shoreline reconstruction is very similar to that in Fig. 4C for 14,000 years ago, with minimum elevations of the sill less than about 10 m above the coeval sea level. This connection may have broken up briefly at around 37,000 years ago, but otherwise the eastern land route remained effectively above sea level from about 43,000 years ago until 14,000 years ago. The coincidence of the earlier date with the earliest occupation of Warreen Cave suggests that this was probably the time when humans first crossed the Bass Strait.

References and Notes

1. A. Hallam, *Annu. Rev. Earth Planet. Sci.* **12**, 205 (1984).
2. P. R. Vail, J. Hardenbol, R. G. Todd, *Am. Assoc. Petrol. Geol. Mem.* **36**, 129 (1984).
3. M. Nakada, K. Lambeck, *Nature* **33**, 36 (1988).
4. A. M. Tushingham, W. R. Peltier, *J. Geophys. Res.* **96**, 4497 (1991).
5. W. R. Peltier, *Rev. Geophys.* **36**, 603 (1998).
6. P. J. Johnston, K. Lambeck, *J. Geophys. Res.* **105**, 13179 (2000).
7. J. X. Mitrovica, W. R. Peltier, *Geophys. Res. Lett.* **19**, 1185 (1992).
8. K. Lambeck, C. Smither, P. Johnston, *Geophys. J. Int.* **134**, 102 (1998).
9. K. Lambeck, *Geophys. J. Int.* **122**, 1022 (1995).
10. J. A. Church *et al.*, *Intergovernmental Panel on Climate Change Third Assessment Report* (Cambridge Univ. Press, in press), chap. 11.
11. Corals can provide a precise indicator of sea level when the colony lives up to the mean low sea level, as is the case for the micro-atoll formations of some species (*23*, *24*). In other situations, the range of the coral habitat may be as large as 5 to 10 m, and the sea level estimate is correspondingly uncertain (*20*, *21*).
12. K. D. Vorren, D. Moe, *Norsk Geol. Tidd.* **66**, 135 (1986).
13. R. Lidén, *Geol. Foren. Furhandl.* **60**, 397 (1938). These results have been cross-checked with isolation basin results to ensure consistency between the different sea levels.
14. A. Heyworth, C. Kidson, *Proc. Geol. Assoc.* **93**, 91 (1982).
15. T. Hanebuth, K. Stattegger, P. M. Grootes, *Science* **288**, 1033 (2000). The majority of the core samples are from the vicinity of the islands of Natuna Besar, between the Malay Peninsula and Kalimantan.
16. R. G. Fairbanks, *Nature* **342**, 637 (1989).
17. E. Bard, B. Hamelin, R. G. Fairbanks, *Nature* **346**, 456 (1990).
18. E. Bard, M. Arnold, R. G. Fairbanks, B. Hamelin, *Radiocarbon* **35**, 191 (1993).
19. See E. Bard *et al.*, *Nature* **382**, 241 (1996) for similar results from Tahiti and see (*30*) for similar results from Huon Peninsula, Papua New Guinea.
20. R. G. Lighty, I. C. Macintyre, R. Stuckenrath, *Coral Reefs* **1**, 125 (1982).
21. L. Montaggioni *et al.*, *Geology* **25**, 555 (1997).
22. E. Bard, M. Arnold, B. Hamelin, N. Tisnerat-Laborde, G. Cabioch, *Radiocarbon* **40**, 1085 (1998).
23. J. Chappell, *Nature* **302**, 406 (1983).
24. C. Woodroffe, R. McLean, *Nature* **344**, 531 (1990).
25. A. S. Dyke, T. F. Morris, D. E. C. Green, *Geol. Surv. Can. Bull.* **397**, 56 (1991).
26. I. Shennan *et al.*, *Quat. Sci. Rev.* **19** 1103 (2000).
27. Y. Yokoyama, K. Lambeck, P. De Deckker, P. Johnston, L. K. Fifield, *Nature* **406**, 713 (2000).
28. J. Chappell, A. Chivas, E. Wallensky, H. A. Polach, P. Aharon, *Bur. Min. Res. J. Geol. Geophys.* **8**, 223 (1983).
29. K. Lambeck, M. Nakada, *Palaeogeogr. Palaeoclim. Palaeoecol.* **89**, 143 (1990).
30. J. Chappell, H. Polach, *Nature* **349**, 147 (1991).
31. R. L. Edwards *et al.*, *Science* **260**, 962 (1993).
32. J. Chappell, Y. Ota, K. Berryman, *Quat. Sci. Rev.* **15**, 7 (1996).
33. J. Chappell *et al.*, *Earth Planet. Sci. Lett.* **141**, 227 (1996).
34. T. M. Esat, M. T. McCulloch, J. Chappell, B. Pillans, A. Omura, *Science* **283**, 197 (1999).
35. Y. Yokoyama, T. Esat, K. Lambeck, L. K. Fifield, *Radiocarbon* **42**, 383 (2000).
36. K. Lambeck, Y. Yokoyama, A. Purcell, *Quat. Sci. Rev.*, in press.
37. The height-age information for the principal reefs of the Huon Peninsula constrains the pre-LGM sea level curve (Fig. 3A). The intervening lowstands, including that at about 140,000 years ago, have been inferred from the delta sequences of the nearby Tewai section (*38*) and from models of the response of terrace morphology and reef facies to sea level change (*39*).
38. J. Chappell, N. J. Shackleton, *Nature* **324**, 137 (1986).
39. J. Chappell, *Quat. Sic. Rev.*, in press.
40. C. H. Stirling *et al.*, *Science* **291**, 290 (2001).
41. J. Galewsky, E. A. Silver, C. D. Gallup, R. L. Edwards, D. C. Potts, *Geology* **24**, 819 (1996).
42. This is an important feature because the spatial variability of these highstand amplitudes is sensitive to the mantle rheology, whereas the amplitude itself is a function of both rheology and of any residual changes in ice volume at this time. Precise observations of this spatial variability allow the two contributions to be separated (*29*).
43. W. R. Peltier, *Rev. Geophys.* **12**, 649 (1974).
44. W. E. Farrell. J. A. Clark, *Geophys. J. R. Astron. Soc.* **46**, 647 (1976).
45. M. Nakada, K. Lambeck, *Geophys. J. R. Astron. Soc.* **90**, 171 (1987).
46. P. Johnston, *Geophys. J. Int.* **114**, 615 (1993).
47. J. X. Mitrovica, J. L. Davis, I. I. Shapiro, *J. Geophys. Res.* **99**, 7075 (1994).
48. G. A. Milne, J. X. Mitrovica, *Geophys. J. Int.* **133**, 1 (1998).
49. G. A. Milne, J. X. Mitrovica, J. L. Davis, *Geophys. J. Int.* **139**, 464 (1999).
50. K. Lambeck, P. Johnston, in *The Earth's Mantle*, I. Jackson, Ed. (Cambridge Univ. Press, Cambridge, 1998), pp. 461–502.
51. G. Kaufman, K. Lambeck, *Phys. Earth Planet. Int.* **121**, 301 (2000).
52. G. H. Denton, T. J. Hughes, *The Last Great Ice Sheets* (Wiley, New York, 1981).
53. A. Dyke, J. S. Vincent, J. T. Andrews, L. A. Dredge, W. R. Cowan, in *Quaternary Geology of Canada and Greenland*, R. Fulton, Ed. (Geological Survey of Canada, Ottawa, 1989), pp. 178–189.
54. J. Lundquist, *Quat. Sci. Rev.* **5**, 269 (1986).
55. J. I. Svendsen *et al.*, *Boreas* **28**, 234 (1999).
56. G. H. Denton, J. G. Brockheim, S. C. Wilson, M. Stuiver, *Quat. Res.* **31**, 151 (1989).
57. The ice-volume equivalent sea level estimates in Fig. 3, A and B, are based on a variety of previously published and some unpublished results. The results from 125,000 to about 5000 years ago are from sources listed in (*15–19*, *27*, *30–35*, *38, 39, 94*). The record for the past 7000 years is from various sources summarized in (*58*). The isostatic corrections $\Delta\zeta_i + \Delta\zeta_w$ in Eq. 4 are based on response parameters that have been found to be appropriate for continental margin response with lower upper mantle viscosity for ocean response for the islands of Tahiti and Barbados (Table 1). Tectonic movements have been removed where appropriate, using the elevation of the Last Interglacial shorelines as a measure of average vertical movement. Error estimates, including an assessment of the relationship between the sea level indicators and mean sea level, uncertainties in the tectonic corrections, and the effect of age uncertainty on the latter corrections, as well as uncertainties in the model predictions of the isostatic corrections, are discussed in (*33*). Error bars for the individual estimates in Fig. 3B are not shown but are similar in amplitude to the range of values obtained from the different records.
58. K. Lambeck, in *Glacial Isostatic Adjustment and the Earth System*, J. X. Mitrovica, L. L. A. Vermeersen, Eds. (American Geophysical Union, Washington, DC, in press).
59. P. Huybrechts, *Ann. Glaciol.* **20**, 336 (1994).
60. E. Bard, *Science* **284**, 1133 (1999).
61. G. Bond *et al.*, *Nature* **365**, 143 (1993).
62. M. Bender *et al.*, *Nature* **372**, 663 (1994).
63. D. Zwartz *et al.*, in *The Antarctic Region: Geological Evolution and Processes*, C. Ricci, Ed. (Terra Antarctica Publications, Sienna, Italy, 1997), pp. 821–828.
64. M. Nakada *et al.*, *Mar. Geol.* **167**, 85 (2000).
65. K. Lambeck, Y. Yokoyama, P. Johnston, A. Purcell, *Earth Planet. Sci. Lett.* **181**, 513 (2000).
66. CLIMAP Project Members, *Geol. Soc. Am. Map Chart Ser.* **MC-36**, 1 (1981).
67. D. P. Schrag, G. Haupt, D. W. Murray, *Science* **272**, 1930 (1996).
68. N. J. Shackleton, *Science* **289**, 1897 (2000).
69. M. Stuiver, P. Grootes, *Quat. Res.* **53**, 277 (2000).
70. The ongoing sea level fall at Ångerman or Andøya (Fig. 2), for example, indicates an ongoing response of the earth long after all ice vanished over Scandinavia at 9000 years ago.
71. J. X. Mitrovica, *J. Geophys. Res.* **101**, 555 (1996).
72. K. Lambeck, *Tectonophysics* **223**, 15, (1993).
73. _____ *et al.*, *Geophys. J. Int.* **125**, 340 (1996).
74. M. Nakada, K. Lambeck, *Geophys. J. Int.* **96**, 497 (1989).
75. A. M. Forte, J. X. Mitrovica, *Geophys. Res. Lett.* **23**, 1147 (1996).
76. B. H. Hager, *J. Geophys. Res.* **89**, 6003 (1984).
77. Y. Ricard, M. Richards, C. Lithgow-Bertelloni, Y. Le Stunff, *J. Geophys. Res.* **94**, 21895 (1993).
78. B. Romanowicz, *Pure Appl. Geophys.* **153**, 257 (1998).
79. This approach assumes that a major part of the rebound or sea level change is determined by the

regional mantle response. For sites far from the ice sheets, the primary contribution is from the regional response to the change in water load, although there remains a component of global flow in response to the distant glacial unloading, and the resulting viscosity estimate will partly reflect mantle conditions beneath the ice sheets. Likewise, for sites near the rebound centers, the response will be largely determined by the mantle beneath the ice load, but there will remain a smaller component that is determined by mantle conditions further away. Thus, although the regional results should indicate whether lateral variation is likely to be important, they will not lead to definitive values.

80. M. Nakada, K. Lambeck, in *Glacial Isostasy, Sea-level and Mantle Rheology*, R. Sabadini, K. Lambeck, E. Boschi, Eds. (Kluwer, Dordrecht, Netherlands, 1991), pp. 79–94.
81. W. R. Peltier, *Science* **265** 195 (1994).
82. K. Lambeck, *J. Geol. Soc. London* **152**, 437 (1995).
83. _____, *Antiquity* **70**, 588 (1996).
84. _____, *Earth Planet. Sci. Lett.* **142**, 43 (1996).
85. T. W. Jacobson, *Sci. Am.* **234**, 343 (1976).
86. T. H. van Andel, in *Landscapes and People of the Franchthi Region*, T. W. Jacobson, Ed. (Indiana Univ. Press, Bloomington, IN, 1987), pp. 3–64.
87. G. Roux, *Ancient Iraq* (Penguin, London, 1992).
88. G. Roux, in *Initiation in l'Orient Ancien*, J. Bottéro, Ed. (Editions du Seuil, Paris, 1992), pp. 37–56.
89. R. Jones, *Annu. Rev. Anthropol.* **24**, 423 (1995).
90. R. Cosgrove, J. Allen, B. Marshall, *Antiquity* **64**, 59 (1990).
91. J. F. O'Connell, J. Allen, *Evol. Anthropol.* **6**, 132 (1998).
92. A. Thorne *et al.*, *J. Hum. Evol.* **36**, 591 (1999).
93. R. Grün *et al.*, *J. Hum. Evol.* **38**, 733 (2000).
94. J. Gibb, *R. Soc. N. Z. Bull.* **24**, 377 (1986).
95. P. L. Woodworth *et al.*, *Geophys. J. Int.* **136**, 651 (1999).
96. M. Ekman, *Global Planet. Change* **21**, 215 (1999).

REVIEW

Trends, Rhythms, and Aberrations in Global Climate 65 Ma to Present

James Zachos,[1]* Mark Pagani,[1] Lisa Sloan,[1] Ellen Thomas,[2,3] Katharina Billups[4]

Since 65 million years ago (Ma), Earth's climate has undergone a significant and complex evolution, the finer details of which are now coming to light through investigations of deep-sea sediment cores. This evolution includes gradual trends of warming and cooling driven by tectonic processes on time scales of 10^5 to 10^7 years, rhythmic or periodic cycles driven by orbital processes with 10^4- to 10^6-year cyclicity, and rare rapid aberrant shifts and extreme climate transients with durations of 10^3 to 10^5 years. Here, recent progress in defining the evolution of global climate over the Cenozoic Era is reviewed. We focus primarily on the periodic and anomalous components of variability over the early portion of this era, as constrained by the latest generation of deep-sea isotope records. We also consider how this improved perspective has led to the recognition of previously unforeseen mechanisms for altering climate.

Through study of sedimentary archives, it has become increasingly apparent that during much of the last 65 million years and beyond, Earth's climate system has experienced continuous change, drifting from extremes of expansive warmth with ice-free poles, to extremes of cold with massive continental ice-sheets and polar ice caps. Such change is not unexpected, because the primary forces that drive long-term climate, Earth's orbital geometry and plate tectonics, are also in perpetual motion. Much of the higher frequency change in climate (10^4 to 10^5 years) is generated by periodic and quasi-periodic oscillations in Earth's orbital parameters of eccentricity, obliquity, and precession that affect the distribution and amount of incident solar energy (Fig. 1) (*1*). Whereas eccentricity affects climate by modulating the amplitude of precession and thus influencing the total annual/seasonal solar energy budget, obliquity changes the latitudinal distribution of insolation. Because the orbital parameters vary with distinct tempos that remain stable for tens of millions of years (*2*), they provide a steady and, hence, predictable pacing of climate.

The orbitally related rhythms, in turn, oscillate about a climatic mean that is constantly drifting in response to gradual changes in Earth's major boundary conditions. These include continental geography and topography, oceanic gateway locations and bathymetry, and the concentrations of atmospheric greenhouse gases (*3*). These boundary conditions are controlled largely by plate tectonics, and thus tend to change gradually, and for the most part, unidirectionally, on million-year (My) time scales. Some of the more consequential changes in boundary conditions over the last 65 My include: North Atlantic rift volcanism, opening and widening of the two Antarctic gateways, Tasmanian and Drake Passages (*4*); collision of India with Asia and subsequent uplift of the Himalayas and Tibetan Plateau (*5*); uplift of Panama and closure of the Central American Seaway (*6*) (Figs. 1 and 2); and a sharp decline in pCO_2 (*7*). Each of these tectonically driven events triggered a major shift in the dynamics of the global climate system (*8–15*). Moreover, in altering the primary boundary conditions and/or mean climate state, some or all of these events have altered system sensitivity to orbital forcing (*16*), thereby increasing the potential complexity and diversity of the climate spectrum. This would include the potential for unusually rapid or extreme changes in climate (*17, 18*).

Although Earth's climatic history has been reconstructed with an array of proxies applied to both marine and terrestrial sediment archives, much of the progress in resolving the rates and scales of Cenozoic climate change can be attributed to the development of high-resolution deep-sea oxygen ($\delta^{18}O$) and carbon ($\delta^{13}C$) isotope records (*19*). Since the early 1970s, $\delta^{18}O$ data have served as the principal means of reconstructing global and regional climate change on a variety of geologic time-scales, from millennial to tectonic. These records are multidimensional in that they provide both climatic and stratigraphic information, and can be quickly generated with automated mass spectrometers. The first marine isotope records were relatively coarse, but still provided valuable insight into the general structure of the Pleistocene glacial and interglacial cycles (*20*). These were followed by records delineating the long-term patterns of Cenozoic climate change (*21–23*) and, eventually, the first global compilation of records for the Cenozoic (resolution of 10^5 to 10^6 years) (*24*).

The last decade has witnessed a rapid growth in the inventory of high-resolution isotope records across the Cenozoic, aided by the greater availability of high-quality sediment cores recovered by the Deep Sea Drilling Project (DSDP) and Ocean Drilling Program (ODP). The improved perspective provided by these records has led to some of the most exciting scientific developments of the

[1]Earth Sciences Department, University of California, Santa Cruz, CA 95064, USA. [2]Department of Earth and Environmental Sciences, Wesleyan University, Middletown, CT 06459, USA. [3]Center for the Study of Global Change, Yale University, New Haven, CT 06520–8105, USA. [4]College of Marine Studies, University of Delaware, Lewes, DE 19958, USA.

*To whom correspondence should be addressed. E-mail: jzachos@es.ucsc.edu